Magnetic Resonance in Medicine 50:493–499 (2003)

Equilibrium Water Exchange Between the Intra- and Extracellular Spaces of Mammalian Brain

James D. Quirk,[1] G. Larry Bretthorst,[1] Timothy Q. Duong,[1] Avi Z. Snyder,[2] Charles S. Springer, Jr.,[3,4] Joseph J.H. Ackerman,[1,2,5] and Jeffrey J. Neil[2,6*]

This report describes the measurement of water preexchange lifetimes and intra/extracellular content in intact, functioning mammalian brain. Intra- and extracellular water magnetic resonance (MR) signals from rat brain in vivo were quantitatively resolved in the longitudinal relaxation domain following administration of an MR relaxation agent into the extracellular space. The estimated intracellular water content fraction was 81% ± 8%, and the intra- to extracellular exchange rate constant was 1.81 ± 0.89 s^{-1} (mean ± SD, N = 9), corresponding to an intracellular water preexchange lifetime of ~550 ms. These results provide a temporal framework for anticipating the water exchange regime (fast, intermediate, or slow) underlying a variety of compartment-sensitive measurements. The method also supplies a means by which to evaluate membrane water permeability and intra/extracellular water content serially in intact tissue. The data are obtained in an imaging mode that permits detection of regional variations in these parameters. Magn Reson Med 50:493–499, 2003. © 2003 Wiley-Liss, Inc.

Key words: water exchange; brain; magnetic resonance; membrane permeability; cell water content

Knowledge of the rate constants governing exchange or, equivalently, the preexchange lifetime (or residence time) of water in the intra- and extracellular compartments of the mammalian brain would be extremely valuable for interpreting a wide range of magnetic resonance (MR) experiments. When compartment-sensitive MR measurements of water properties are made, the proper interpretation of experimental results requires a clear understanding of the governing exchange regime. This exchange regime is a function of the time scale of the experiment and the residence lifetimes of the molecule of interest in the relevant compartments. If the experimental time scale is long relative to the residence lifetime, the system is in fast exchange and observations reflect a dynamic averaging of compartment properties. If the experimental time scale is short relative to the residence lifetime, the system is in slow exchange and compartmental signals can be analyzed separately. For instance, considerable controversy currently exists as to the mechanism(s) underlying the change in water apparent diffusion coefficients (ADCs), which provide remarkable contrast in diffusion-weighted brain imaging (1). To better understand this contrast, it would be very useful to make intra- and extracellular compartment-specific measurements of water diffusion. However, it is not possible to obtain such measurements unless the water exchange regime (fast, slow, or intermediate) relevant to the study is understood.

In order to measure this exchange, one must discriminate between MR signals arising from water in the intra/extracellular compartments. Were such discrimination possible, it would open the way for measurement not only of water preexchange lifetime and membrane permeability, but also the relative water content fractions of the two compartments. The relative water content fraction is believed to change under conditions of cell swelling and/or shrinkage, such as occurs with cell injury. In the study described below, we estimated the intra/extracellular water content ratios, water exchange rate constants, and membrane water permeability in intact mammalian brain.

In theory, there are at least three ways to discriminate MR signal arising from different tissue compartments. One is based on chemical shift or resonance frequency. However, the ^{1}H resonance of water does not have a discernible resonance frequency difference between the intra- or extracellular spaces. In principle, it is possible to administer a chemical shift reagent to one compartment, shifting the resonance frequency of the species of interest. To date, however, no practical chemical shift reagent has been developed for the ^{1}H resonance of water.

A second means of achieving compartmental discrimination is based on transverse (or R_2 and R_2^*) ^{1}H relaxation [$R_2 \equiv (T_2)^{-1}$] (2). However, it is likely that R_2 and R_2^* MR relaxation rate constants for water are similar (and possibly nonuniform (3–5)) for the intra- and extracellular spaces. While MR relaxation agents are available to alter R_2 and R_2^* relaxation rate constants, they also introduce magnetic susceptibility gradients which cross compartmental boundaries. As a result, the presence of relaxation agent in the extracellular space reduces the R_2 and R_2^* of both extra- and intracellular water. Thus, R_2 changes may not be sufficiently spatially localized to discriminate between the intra- and extracellular spaces.

[1]Department of Chemistry, Washington University, St. Louis, Missouri.

[2]Department of Radiology, Washington University School of Medicine, St. Louis, Missouri.

[3]Chemistry Department, Brookhaven National Laboratory, Upton, New York.

[4]Department of Chemistry, State University of New York, Stony Brook, New York.

[5]Department of Internal Medicine, Washington University School of Medicine, St. Louis, Missouri.

[6]Division of Pediatric Neurology, Department of Neurology, Washington University, St. Louis, Missouri.

Grant sponsor: NIH; Grant numbers: NS35912; GM32125; NS40801; CA83060.

James D. Quirk's current address is Pfizer Global Research and Development, 700 Chesterfield Parkway West, Chesterfield, MO 63017.

Timothy Q. Duong's current address is Department of Psychiatry, University of Massachusetts Medical School, Worcester, MA 01655.

Charles S. Springer, Jr.'s current address is Advanced Imaging Research Center, Oregon Health & Science University, Portland, OR 97201.

*Correspondence to: Jeffrey J. Neil, Biomedical MR Lab, Campus Box 8227, Washington University School of Medicine, 4525 Scott Ave., Room 2313, St. Louis, MO 63110. E-mail: neil@wuchem.wustl.edu

Received 9 August 2002; revised 13 March 2003; accepted 21 April 2003.

DOI 10.1002/mrm.10565

Published online in Wiley InterScience (www.interscience.wiley.com).

A third method for discriminating between compartments, which was employed in the current study, is based on longitudinal (or R_1) relaxation ($R_1 \equiv (T_1)^{-1}$). The administration of relaxation agent into the extracellular space results in differences in water ^{1}H MR R_1 relaxation rate constants for the two compartments that are sufficient to resolve signals from the compartments in the relaxation time domain. Once this difference in R_1 relaxation rate constants has been achieved, inversion recovery MR data can be modeled as arising from a two-compartment (intra- and extracellular) system in which water exchange modulates the observed relaxation behavior. The exchange of water between two (relaxation-distinct) compartments results in biexponential magnetization recovery, characterized by "apparent" R_1 values and water population fractions for the two compartments. These values deviate from the "true" values (those that would be observed in the absence of exchange). However, Bloch-McConnell exchange modeling (6–9) can be used to extract exchange-independent relaxation rate constants, the preexchange lifetimes of water molecules in each compartment (from which the cell membrane water diffusional permeability can be calculated (10,11)), and the true water content of the intra- and extracellular spaces.

Under ordinary circumstances, the R_1 relaxation rate constants for water in these compartments are too similar to allow separation on this basis. In this study, the R_1 of extracellular water was markedly increased through the administration of an MR relaxation agent, Gd-DTPA, directly into the brain extracellular space via intracerebroventricular infusion. Gd-DTPA is typically used in clinical protocols in which MRI scans are obtained after its intravenous administration. The agent does not ordinarily cross the blood–brain barrier (BBB) in significant concentrations, and for MR images of the "normal" brain, its R_1 relaxation enhancement is present primarily within blood vessels. In regions in which the BBB is no longer intact, such as regions of tumor or inflammation, the agent crosses and enters the brain. These regions appear bright on T_1-weighted images because the relaxation agent increases the R_1 relaxation rate constant of local water. Thus, when administered in the clinical setting, Gd-DTPA serves as an indicator of BBB breakdown. For the experiments described here, we infused the agent on the *brain* side of the BBB by injecting it directly into the lateral cerebral ventricles.

METHODS

All experiments were approved by the University Animal Studies Committee, Washington University. Nine male Sprague-Dawley rats (290–310 g) were anesthetized with urethane (1.6 g/kg administered intraperitoneally). Two holes (each 1.5 mm in diameter) were drilled into the skull, and two 23-gauge stainless steel needles were simultaneously placed stereotaxically into the lateral ventricles at the coordinates: ±1.4 mm lateral to bregma, 0.8 mm posterior to bregma, and 3.4 mm deep from the dural surface. Then 125 mM Gd-diethylenetriamine pentaacetic acid (Gd-DTPA, Magnevist®; Berlex Laboratories) was infused at 10 μl/hr into each ventricle for 2 hr using a Harvard Apparatus infusion pump, providing a total of 20 μl into each lateral ventricle. Following the infusion, the rat was kept in the stereotaxic headframe, with the needles in place for an additional hour to facilitate distribution of the relaxation agent. All of the animals tolerated the infusion well, without seizures or evidence of brain herniation.

After the relaxation agent was infused, the rats were positioned with the head in the center of a 3-cm quadrature birdcage coil for MRI on a 4.7-T, 40-cm clear-bore, Oxford Instruments magnet and a Varian $^{\text{UNITY}}$INOVA console with 600 mT/m Magnex gradient inserts. T_1-weighted spin-echo images of the rat brains were collected to verify wide distribution of the relaxation agent by evaluating areas of these images that had high signal intensity, reflecting the presence of relaxation agent. This distribution typically required an additional delay of 1–2 hr to achieve. The spin-echo images were collected with a repetition time (TR) of 340 ms, and an echo time (TE) of 12 ms, for 20 coronal slices, each with a $3 \times 3 \times 0.1$ cm^3 field of view (FOV) and 64×64 image matrix. Periodically, T_1-weighted spin-echo images were also collected in the sagittal plane with 13 slices over a $5 \times 3 \times 0.1$ cm^3 FOV, and in the axial plane with nine slices over a $3 \times 3 \times 0.1$ cm^3 FOV. When the relaxation agent appeared widely distributed, inversion-recovery R_1 curves were collected as a series of single-slice, single-shot, coronal EPI images over a $3 \times 6 \times 0.2$ cm^3 FOV. The FOV in the phase-encoding direction was widened to avoid overlap between the N/2 ghosts and the primary image. The EPI images were collected fully relaxed, with a TR of 8 s, and at 64 exponentially-spaced inversion times ranging from 5 ms to 5 s following a 100-μs non-spatially-selective square inversion pulse. Each 64-point inversion recovery data set required approximately 9 min to acquire. This process was repeated 20 times as the relaxation agent was slowly eliminated from the brain. (Repeating the inversion recovery curves at slowly diminishing levels of relaxation agent provided sufficient data for the parameter fittings, as described below.)

The EPI images were coaligned to account for animal motion and gradient instabilities. The image intensities were recorded for each pixel in a region of interest (ROI) encompassing parts of the thalamus and striatum. The rate constants of interest were inferred from each pixel independently using Bayesian probability theory and Markov Chain Monte Carlo integration. The values for all selected pixels from all rats were averaged to produce the final estimates.

The two-site exchange-modified Bloch equations can be described, after McConnell (6), as:

$$\frac{dM_{za}}{dt_{ir}} = -(M_{za} - M_{za\,eq})R_{1a} - M_{za}\,k_{ab} + M_{zb}\,k_{ba} \qquad [1]$$

and

$$\frac{dM_{zb}}{dt_{ir}} = -(M_{zb} - M_{zb\,eq})R_{1b} + M_{za}\,k_{ab} - M_{zb}\,k_{ba} \qquad [2]$$

where M_{za} and M_{zb} are the time-dependent water ^{1}H longitudinal (i.e., z-axis) magnetizations of the intra- and ex-

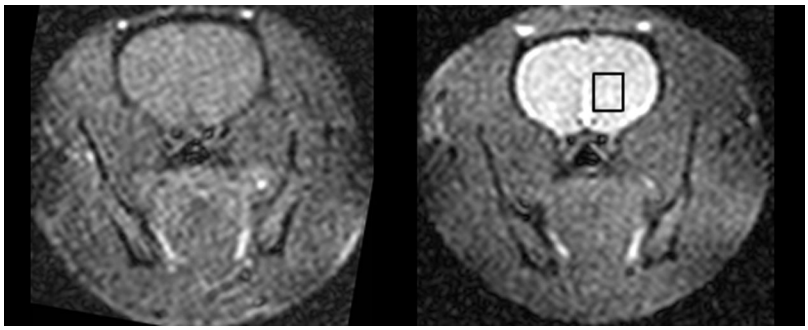

FIG. 1. Coronal T_1-weighted images of the rat head before (left) and after (right) intracerebroventricular infusion of Gd-DTPA. Note the marked increase in signal intensity in brain after the infusion. Because of partial voluming effects, this increase is especially noticeable in CSF-containing spaces of the subarachnoid space. Based on a temporal series of T_1-weighted coronal images (not shown), the initially tightly-localized region of high signal intensity (corresponding to a relatively high Gd-DTPA concentration) appeared to disperse widely within 4 hr of the infusion. The rectangle on the image on the right represents the ROI from which voxels were chosen for parameter estimation.

tracellular compartments, respectively. The additional "*eq*" subscripts refer to equilibrium magnetization, i.e., that at $t = \infty$. R_{1a} and R_{1b} are the true R_1 spin lattice or longitudinal relaxation rate constants for the two compartments—the values that would be present in the absence of exchange. The parameters k_{ab} and k_{ba} are the rate constants for exchange from the intra- to extracellular space and extra- to intracellular space, respectively. The parameter t_{ir} represents time after the RF inversion pulse. The two coupled, linear, first-order, inhomogeneous differential equations were solved for:

$$M_z(t) = M_{zb}(t) + M_{za}(t). \quad [3]$$

The washout of the relaxation agent from the interstitial space was also estimated based on the expression

$$R_{1b} = R^0_{1b} + (R^{initial}_{1b} - R^0_{1b})e^{-t_{washout}R_{washout}} \quad [4]$$

Note that the time scale for this expression is different from that in Eqs. [1] and [2]. For Eq. [4], the time scale is that of the washout of tracer from the extracellular space, and $t_{washout}$ represents the time after infusion and distribution of the relaxation agent. For Eqs. [1] and [2], the time scale is that of recovery of *z*-axis magnetization following the inversion RF pulse (hence the use of t_{ir} for time in those expressions). $R_{1b}(t_{washout})$ remains the true R_1 relaxation rate constant for extracellular water, R^0_{1b} is the extracellular water R_1 relaxation rate constant in the absence of relaxation agent, $R^{initial}_{1b}$ is the starting R_1 relaxation rate constant of extracellular water after the infusion of relaxation agent (i.e., at the highest concentration of relaxation agent), and $R_{washout}$ is the rate constant for tracer washout.

The entire inversion recovery data set (i.e., 64 t_{ir} periods × 20 inversion recovery experiments × ~50 voxels/rat) was analyzed using the solution to Eqs. [1], [2], and [4] by employing Bayesian probability theory. The prior information used in the computation was: 1) the water content in the two pools was at equilibrium and thus, by the condition of microscopic reversibility,

$$\frac{M_{zb\,eq}}{M_{za\,eq}} = \frac{k_{ab}}{k_{ba}}, \quad [5]$$

2) the rate constants (k and R_1) were greater than or equal to zero, and 3) the inversion pulse affected water magnetization in both compartments identically. Thus,

$$M_{zb}(0) = -\rho M_{zb\,eq} \quad [6]$$

and

$$M_{za}(0) = -\rho M_{za\,eq} \quad [7]$$

where $\rho = 1$ for an ideal inversion. Note that the value for ρ need not be unity, or even known, so long as it is the same locally for intra- and extracellular water. For each individual voxel in a given animal, the 20 inversion recovery data sets were analyzed jointly. In each animal, the ROI encompassed approximately 50 voxels, for a total of 455 voxels from nine rats. Markov Chain Monte Carlo (12) was employed to draw samples from the joint marginal posterior distribution for decay and exchange parameters (the amplitudes were removed using the sum rule of probability theory). These sample values were used to approximate the marginal distribution for each of the parameters. The means and standard deviations (SDs) of these samples were calculated to provide estimates of each of the following parameters for water: intra- to extracellular (k_{ab}) and extra- to intracellular (k_{ba}) exchange rate constants, intracellular ^1H_2O R_1 relaxation rate constant in the absence of exchange (R_{1a}), extracellular ^1H_2O R_1 relaxation rate constant in the absence of exchange at the highest concentration of contrast agent ($R^{initial}_{1b}$), extracellular ^1H_2O R_1 relaxation rate constant in the absence of relaxation agent (R^0_{1b}), and the washout rate constant for the elimination of Gd-DTPA from the brain ($R_{washout}$). For more details on the methods used for the parameter estimates, see Refs. 13 and 14.

RESULTS

We were able to follow the dissemination of the relaxation agent throughout the nervous system using T_1-weighted

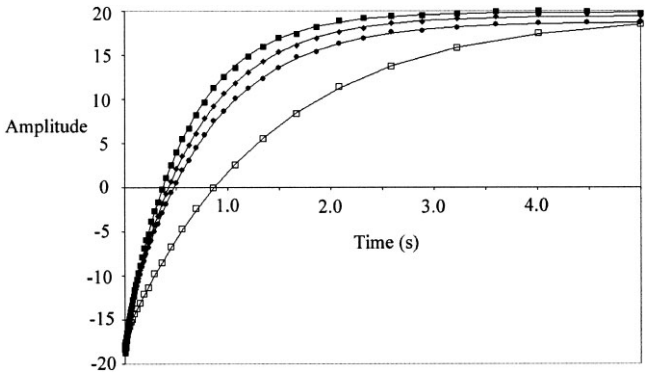

FIG. 2. Magnetization inversion-recovery curves obtained from the entire ROI of rat brain before (open squares) and after intracerebroventricular administration of 125 mM Gd-DTPA. Note that the recovery rate is much faster after the addition of the relaxation agent to the extracellular space. Curves were obtained immediately after wide distribution of infused Gd-DTPA (filled squares), 90 min later (filled diamonds), and 180 min later (filled circles). A total of 20 curves was obtained from each animal; for clarity, only three representative curves are shown. Note that the relaxation rate decreases as the relaxation agent washes out of the brain. Bayesian analysis employing an exponential signal expression indicated that the data obtained from each voxel prior to the infusion of relaxation agent were generally well modeled by a monoexponential function, while those obtained after infusion were well modeled with a biexponential function. This suggests that the R_1 values for water in the two compartments are too similar to be distinguished without the administration of relaxation agent. The addition of relaxation agent has the effect of moving the inversion recovery experiment from the fast-exchange regime (without contrast agent, monoexponential recovery) to intermediate exchange (with contrast agent, biexponential recovery). The line through the curve obtained before infusion represents the Bayesian parameter estimates using a simple monoexponential model. The lines through the curves obtained after infusion represent the two-site exchange model with the optimally-estimated parameter values. The parameter estimates were taken from the means of the probability distribution functions.

imaging, as shown in Fig. 1. It was widely distributed by approximately 1–2 hr after the end of the infusion. The concentration of Gd-DTPA used for this study was the maximum dose tolerated well by the animal. This was done in order to maximize the difference in R_1 values between intra- and extracellular space. Typical inversion recovery curves are shown in Fig. 2.

The priors used for Bayesian analysis are shown in Table 1. The parameters estimated are 82% ± 8% (mean ± SD) for intracellular water content fraction, 1.81 ± 0.89 s^{-1} for the rate constant governing exchange from the intra- to extracellular space (corresponding to a ~550 ms intracellular water preexchange lifetime), and 8.5 ± 4.8 s^{-1} for the rate constant governing exchange from the extra- to intracellular space (corresponding to a ~120 ms extracellular water preexchange lifetime).

Values of the rate constant for washout of relaxation agent from the extracellular space were distributed asymmetrically, with a mean value of 0.02 ± 0.05 min^{-1}. The spin lattice relaxation rate constant for extracellular ^1H_2O in the absence of Gd-DTPA was 12.4 ± 12.6 s^{-1}. The intracellular ^1H_2O relaxation rate constant (R_{1a}) was relatively poorly determined, with the data indicating that it is <0.22 s^{-1} (vide infra).

DISCUSSION

The key finding of this study is the preexchange lifetimes for intra- and extracellular water in intact mammalian brain, which are ~550 and 120 ms, respectively. These lifetimes are of paramount importance for experiments in which compartment-specific properties of water are evaluated. This study provides the necessary information by which the exchange time scale of a given experiment (slow, intermediate, or fast) can be determined. To our knowledge, this is the first accurate measurement of these lifetimes in intact brain. Investigators have generally assumed preexchange lifetimes on the order of those found in red blood cells (i.e., ~10 ms). Our data indicate that the lifetime is an order of magnitude longer.

The data obtained were analyzed according to the Bloch-McConnell, two-compartment exchange model (6–9). This model is commonly used to measure the kinetic rate constants governing exchange between different resonance-frequency-resolved molecular species or sites detected by high-resolution, solution-state NMR (see, for example, Ref. 15). The presence of two (or more) separate resonance frequencies allows selective magnetization inversion (or saturation) at each molecular site, followed by separate measurement of their respective magnetization amplitudes as the system returns (relaxes) toward equilibrium. In the case of the experiments described herein, the exchange takes place between different water compartments rather than different molecular species, and the water ^1H signals from the two compartments have the same resonance frequency. This significantly complicates the data analysis because water ^1H magnetization in the two compartments must be inverted simultaneously, and it is not possible to determine the magnetization amplitudes of the two compartments individually—only their sum. However, it is still possible to analyze the relaxation data using the Bloch-McConnell exchange model and estimate the desired parameters. We did this using Bayesian probability theory. One of the powerful features of this method is that it allows for the inclusion of "prior information" in the analysis in the form of the data model used, and as prior probabilities for the parameters to be estimated. These "priors" can influence the parameter estimates, and thus they must be chosen carefully. We chose very broad priors that were within the range of physiologic possibility (Ta-

Table 1
Priors Used for Data Analysis*

Parameter (units)	Low	Mean	High	SD
k_{ab} (s^{-1})	0	5	300	20
k_{ba} (s^{-1})	0	10	300	20
R_{1a} (s^{-1})	0	0.75	50	5
R^0_{1b} (s^{-1})	0	1	50	5
Initial R_{1b} (s^{-1})	0	20	150	20
$R_{washout}$ (min^{-1})	0	0.05	1	0.5

*These priors are Gaussian functions with the indicated means and SDs. They are truncated to zero at the low and high limits.

ble 1). We also ran a series of simulations on computer-generated data and used different priors to ensure that the parameter estimates obtained for this study were determined by the data and not overly influenced by the prior probabilities (data not shown). Another advantage of this method is that the parameter estimates are cast in the form of a probability density function (PDF). The PDF provides information on the uncertainty in the estimate for a given data set. As discussed below, these PDFs can be asymmetric, indicating an asymmetric likelihood for parameter values greater or less than the most likely parameter value.

The value of ~82% obtained for the intracellular water content fraction is quite close to whole-brain average values obtained using more conventional methods (16,17). Note that the values represented here are not volume fractions, but rather the compartmental fractions of total water in each compartment. For an intracellular water fraction of 0.82, the corresponding cell volume fraction is 0.84 if the 20% of tissue volume that is nonaqueous is apportioned completely to the cell volume fraction.

It is interesting to note that our estimate of intracellular preexchange lifetime (550 ms) is quite different from that reported in Ref. 18 (15 ms). In that study, water ^{1}H MR signal from the intra- and extracellular compartments was separated on the basis of assumed compartmental differences in the ADC. Water with the higher ADC was assigned to the extracellular space. There is evidence that this means of separating signal from these two compartments is ineffective because the water ADC values in the two compartments may be similar (19). To further complicate matters, intracellular water alone has been reported to have multiple ADC components (20,21). If this is the case, it is likely that Pfeuffer et al. (18) reported the exchange rate between other pools of water molecules, potentially pools within the intracellular space. For example, intracellular water that is bound to macromolecules would likely have smaller ADC values than intracellular water that is not bound to macromolecules. These bound and unbound intracellular populations may have been the two compartments studied by Pfeuffer et al. (18), because their discrimination was based on relative ADC values. The preexchange lifetimes of water molecules in these compartments are probably short, as was reported by Pfeuffer et al. (18). We remind the reader that in the present study we employed a relaxation agent to identify the water compartments. The presence of the agent defined the extracellular space, and its absence defined the intracellular space. As can be seen in Table 1, the priors used for our calculation of exchange rate constants included the values proposed in Ref. 18; however, no evidence for this extremely rapid exchange was detected in our data.

The large uncertainty in the estimation of the intracellular ^1H_2O relaxation rate constant (R_{1a}) is because it is small compared to both the exchange rate constants and the GdDTPA-enhanced extracellular water relaxation rate constant. As a result, under the conditions of the experiments reported herein, the main pathway for spin lattice relaxation of intracellular water is exchange to the extracellular compartment and relaxation there, as opposed to relaxation while in the intracellular space. In other words, the spin lattice relaxation of intracellular water is dominated by exchange-coupled relaxation in the extracellular space, and the data contain comparatively little information regarding intracellular R_1. The value provided above for R_{1a} is given without an SD because the distribution of measured values was asymmetric, with a tendency for values below 0.22 s^{-1} to be equally represented. An additional factor contributing to the uncertainty of the parameter estimates was the relatively limited dynamic range for R_{1b} afforded by gradual contrast agent washout during the 3-hr data collection period. The estimate of R_{1b}^0 is itself relatively poorly determined because it represents a significant extrapolation from this low-dynamic-range situation.

It is possible to calculate a value for the membrane water permeability coefficient from the preexchange lifetime using the relationship (10):

$$P = \tau_i^{-1}\left(\frac{V_i}{A}\right) \quad [8]$$

where P is the membrane permeability coefficient, τ_i is the intracellular preexchange lifetime (k_{ab}^{-1}), V_i is the intracellular volume, and A is the cell surface area. If one assumes a typical central nervous system element to be a cell process of diameter ~3 μm (22,23), one obtains a membrane permeability coefficient of 0.10×10^{-3} cm/s. It is important to note that the measurement reported here was made on "brain" cells, because there is as yet no means to separately identify water ^{1}H MR signals arising from neurons and glia. Consequently, the values obtained represent an average of those for the distributed populations of these two cell types (for discussion, see Ref. 24). Further, the value for membrane water permeability reported here is that for "diffusional" permeability rather than "osmotic" permeability. Diffusional permeability refers to the exchange of water molecules across a membrane under conditions in which there is no change in cell size induced by application of an osmotic gradient between the intra- and extracellular spaces. For cells containing membrane water channels, osmotic permeability may be significantly greater than diffusional permeability (25).

There are relatively few values in the literature for diffusional water permeability with which to compare the values obtained in this study. As is apparent from Table 2, these values may vary markedly for various tissue types. One neural tissue type for which values are available is the squid axon. The value of 0.10×10^{-3} cm/s reported in this study is in reasonable agreement with the value of 0.14×10^{-3} cm/s reported for the squid axon (25). In contrast, membrane water permeability for red blood cells—a highly-studied model system—is considerably higher than for nervous tissue. This may be related to the presence of numerous membrane water channels or aquaporins in red blood cells (26). Such channels are also found in the central nervous system, though they appear to be fewer in number. Aquaporin 4 channels, for example, are expressed in osmosensory areas, a localization that suggests a role in osmoregulation (27). The ability to measure diffusional permeability in intact organs, such as the brain, will aid in the evaluation of these membrane channels.

We have described a determination of the rate constants governing water exchange (membrane water permeability)

Table 2
Comparison of Membrane Water Permeability Coefficients of Various Cell Types

Cell type	Intracellular preexchange lifetime (ms)	Membrane water permeability $\times 10^3$ (cm/s)	T (°C)	Reference
Amoeba proteus cell	–	0.021	–	(29)
Rat brain in vivo	500	0.10	37	this study
	15	–	37	(18)
Squid axon	–	0.14	22–24	(25)
Bullfrog sciatic nerve	147	–	20	(30)
Yeast cell	670	0.1	25	(31)
	80–700	0.1–0.8	27	(32)
Rat thigh muscle	1100	1.3	37	(11)
Necturus gallbladder	64	1.6	25	(33)
Renal proximal tubule	12	2.0	25	(34)
Rabbit salivary gland	244	3.0	37	(35)
Human red blood cell	12–22	4.5–8.0	25	(36)
	6–9	11–17	37	(36)

in intact mammalian brain. The compartmental exchange time is defined by $(k_{ab} + k_{ba})^{-1}$, where k_{ab} is the rate constant for intra- to extracellular exchange, and k_{ba} is the rate constant for extra- to intracellular exchange. The rate constant for water exchange from extra- to intracellular space ($k_{ba} \approx 8.5\ s^{-1}$) is significantly greater than that for exchange from intra- to extracellular space ($k_{ab} \approx 1.8\ s^{-1}$). Thus, exchange from extra- to intracellular space dominates the kinetics. Compartment-specific studies of brain water (MR or otherwise) done at a time scale much shorter than approximately 100 ms would therefore be in the slow-exchange regime, whereas those done at time scales much longer should be interpreted in terms of the fast-exchange regime. This is applicable to all studies, MR or otherwise, in which compartment-specific water properties are evaluated. In general, the experimental time scale must be kept short to prevent blurring of properties for water in the two compartments. For example, models of water T_1 relaxation in which relaxation agent enters extracellular, but not intracellular, space from the vascular system should take water exchange into account. This is because water initially in intracellular space would be exposed to the relaxation agent through exchange to the extracellular space, and vice versa. As alluded to above, another important example of a compartment-specific water measurement in brain is the MR determination of water ADCs for intra- and extracellular water (28). For this particular measurement, the experimental time scale is generally determined by the diffusion time, which represents the time interval over which water translational motion is observed. If one wished to allow no more than 10% exchange of water out of the extracellular space during the measurement, a diffusion time on the order of 12 ms [exp(–12 ms/120 ms) = 0.1] would be necessary.

It is worth noting that the apparent imbalance between intra- and extracellular preexchange lifetimes is a consequence of the relative volume fractions of the intra- and extracellular compartments. As can be seen in Eq. [8], the preexchange lifetime is related to the compartment volume, surface area available for exchange, and membrane permeability. If a single cell were placed in a huge volume of water, the preexchange lifetime for intracellular water would be unchanged. This is because the intracellular compartment volume, cell surface area, and membrane permeability are unchanged. The preexchange lifetime for extracellular water, on the other hand, would be extremely long. This is because the extracellular compartment volume would be enormous, with no change in cell surface area or membrane permeability. Given that surface area and membrane permeability are the same for water molecules in the intra- and extracellular spaces, the preexchange lifetime of extracellular water in the brain is shorter than that of intracellular water because the extracellular compartmental volume is smaller.

The current method also provides estimates of the relative amounts of water in the intra- and extracellular spaces. Since an imaging approach was used, it is also possible to determine regional information regarding the parameters described above. In the case of the brain, it was necessary to inject the R_1 relaxation agent directly into the lateral cerebral ventricles to bypass the BBB; however, the method could be generalized to other organs as well. It is possible to administer relaxation agent into the extracellular space of organs lacking a BBB by intravenous infusion (11). In that case, the more rapid elimination of relaxation agent from the extracellular space via renal excretion may prove advantageous in providing a greater relaxation dynamic range than is possible in the brain.

ACKNOWLEDGMENTS

We thank Professor Christopher Sotak for many useful discussions.

REFERENCES

1. Norris DG. The effects of microscopic tissue parameters on the diffusion weighted magnetic resonance imaging experiment. NMR Biomed 2001;14:77–93.
2. Conlon T, Outhred R. Water diffusion permeability of erythrocytes using an NMR technique. Biochim Biophys Acta 1972;288:354–361.
3. Foy BD, Burstein D. Interstitial sodium nuclear magnetic resonance relaxation times in perfused hearts. Biophys J 1990;58:127–134.
4. Rooney WD, Springer Jr CS. The molecular environment of intracellular sodium: ^{23}Na NMR relaxation. NMR Biomed 1991;4:227–245.

5. Ernst T, Kreis R, Ross BD. Absolute quantitation of water and metabolites in the human brain. I. Compartments and water. J Magn Reson B 1993;102:1–8.
6. McConnell HM. Reaction rates by nuclear magnetic resonance. J Chem Phys 1958;28:430–431.
7. Woessner DE. Nuclear transfer effects in nuclear magnetic resonance pulse experiments. J Chem Phys 1961;35:41–48.
8. Leigh JS. Relaxation in systems with chemical exchange: some exact solutions. J Magn Reson 1971;4:308–311.
9. McLaughlin AC, Leigh JS. Relaxation times in systems with chemical exchange: approximate solutions for the nondilute case. J Magn Reson 1973;9:296–304.
10. Chen S-T, Springer Jr CS. Ionophore-catalyzed cation transport between phospholipid inverted micelles manifest in DNMR. Biophys Chem 1981;14:375–388.
11. Landis CS, Li X, Telang FW, Molina PE, Palyka I, Vetek G, Springer Jr CS. Equilibrium transcytolemmal water-exchange kinetics in skeletal muscle in vivo. Magn Reson Med 1999;42:467–478.
12. Gilks WR, Richardson S, Spiegelhalter DJ. Markov Chain Monte Carlo in practice. London: Chapman and Hall; 1996.
13. Quirk JD, Bretthorst GL, Neil JJ. Utilizing MRI to measure the transcytolemmal water exchange rate for rat brain. In: Rychert JT, Erickson GJ, Smith CR, editors. Bayesian inference and maximum entropy methods in science and engineering. New York: American Institute of Physics; 2002. p 285–295.
14. Quirk JD. Compartmental water exchange in the rat brain: a magnetic resonance imaging study. Ph.D. thesis, Washington University, St. Louis, MO, 2001.
15. d'Avignon DA, Bretthorst GL, Holtzer ME, Holtzer A. Site-specific thermodynamics and kinetics of a coiled-coil transition by spin inversion transfer NMR. Biophys J 1998;74:3190–3197.
16. Van Harreveld A. The extracellular space in the vertebrate nervous system. In: Bourne GH, editor. The structure and function of nervous tissue. New York: Academic Press; 1972. p 447–511.
17. van der Toorn A, Sykova E, Dijhuizen RM, Vorisek I, Vargova L, Skobisova E, van Lookeren Campagne M, Reese T, Nicolay K. Dynamic changes in water ADC, energy metabolism, extracellular space volume, and tortuosity in neonatal rat brain during global ischemia. Magn Reson Med 1996;36:52–60.
18. Pfeuffer J, Dreher W, Sykova E, Leibfritz D. Water signal attenuation in diffusion-weighted 1H NMR experiments during cerebral ischemia: influence of intracellular restrictions, extracellular tortuosity, and exchange. Magn Reson Imaging 1998;16:1023–1032.
19. Duong TQ, Ackerman JJH, Ying HS, Neil JJ. Evaluation of extra- and intracellular apparent diffusion in normal and globally ischemic rat brain via ^{19}F NMR. Magn Reson Med 1998;40:1–13.
20. Mulkern RV, Gudbjartsson H, Westin CF, Zengingonul HP, Gartner W, Guttmann CR, Robertson RL, Kyriakos W, Schwartz R, Holtzman D, Jolesz FA, Maier SE. Multi-component apparent diffusion coefficients in human brain. NMR Biomed 1999;12:51–62.
21. Sehy JV, Ackerman JJ, Neil JJ. Evidence that both "fast" and "slow" water ADC components arise from the intracellular space. Magn Reson Med 2002;48:765–770.
22. Szafer A, Zhong J, Gore JC. Theoretical model for water diffusion in tissues. Magn Reson Med 1995;33:697–712.
23. Bok ST. Histonomy of the cerebral cortex. Amsterdam: Elsevier Publishing Company; 1959.
24. Landis CS, Li X, Telang FW, Coderre JA, Micca PL, Rooney WD, Latour LL, Vetek G, Palyka I, Springer Jr CS. Determination of the MRI contrast agent concentration time course in vivo following bolus injection: effect of equilibrium transcytolemmal water exchange. Magn Reson Med 2000;44:563–574.
25. Villegas R, Villegas GM. Characterization of the membranes in the giant nerve fiber of the squid. J Gen Physiol 1960;43:73–104.
26. Verkman AS, Hoek ANV, Tonghui M, Frigeri A, Skach WR, Mitra A, Tamarappoo BK, Farinas J. Water transport across mammalian cell membranes. Am J Physiol 1996;270:C12–C30.
27. Nielsen S, Nagelhus EA, Amiry-Moghaddam M, Bourque C, Agre P, Ottersen OP. Specialized membrane domains for water transport in glial cells: high-resolution immunogold cytochemistry of aquaporin-4 in rat brain. J Neurosci 1997;17:171–180.
28. Silva M, Omae T, Helmer K, Li F, Fisher M, Sotak C. Separating changes in the intra- and extracellular water apparent diffusion coefficient following focal cerebral ischemia in the rat brain. Magn Reson Med 2002;48:826–837.
29. House CR. Water transport in cells and tissues. London: E. Arnold; 1974.
30. Fritz OG, Swift TJ. The state of water in polarized and depolarized frog nerves. Biophys J 1967;7:675–687.
31. Labadie C, Lee J-H, Vetek G, Springer Jr CS. Relaxographic imaging. J Magn Reson 1994;105:99–112.
32. Tanner JE. Intracellular diffusion of water. Arch Biochem Biophys 1983;224:416–428.
33. Steward MC, Garson MJ. Water permeability of *Necturus* gallbladder epithelial cell membranes measured by nuclear magnetic resonance. J Membr Biol 1985;86:203–210.
34. Verkman AS, Wong KR. Proton nuclear magnetic resonance measurement of diffusional water permeability in suspended renal proximal tubules. Biophys J 1987;51:717–723.
35. Steward MC, Seo Y, Rawlings JM, Case RM. Water permeability of acinar cell membranes in the isolated perfused rabbit mandibular salivary gland. J Physiol 1990;431:571–583.
36. Herbst MD, Goldstein JH. A review of water diffusion measurement by NMR in human red blood cells. Am J Physiol 1989;256:C1097–C1104.